Communication

Wideband 3-D-Printed Transmit-Reflect-Array Antenna With Independent Beam Control

Zhenqin Zheng, Long Zhang, Qi Luo, Chunxu Mao, Yejun He, and Steven Gao

***Abstract*— This communication proposes a wideband 3-D-printed transmit-reflect-array (TRA) antenna. The transmission and reflection functions of this TRA antenna are determined by the polarization of the incident electromagnetic wave. The proposed TRA element is composed of a dielectric post and three copper wires, which can be realized by the low-cost 3-D printing. Attributed to the independent control of transmission and reflection phase shift of the proposed element within a wide bandwidth, the proposed TRA antenna can generate two independent transmission and reflection beams over a wide bandwidth. A 12 × 12 TRA is designed, fabricated, and measured to verify the design concept. The measured results show that a peak gain of 24.4 dBi with a bandwidth of 46.8% (18–29 GHz) for the transmitarray (TA) function and a peak gain of 22.9 dBi with a bandwidth of 52.2% (17–29 GHz) for the reflectarray (RA) function are achieved simultaneously by the 3-D-printed TRA antenna. The wide bandwidth, high gain, independent beam control capability, combined TA/RA functions, and low fabrication cost make the proposed antenna appealing for various wireless applications.**

***Index Terms*— 3-D-printed antenna, transmit-reflect-array (TRA) antenna, wideband antenna.**

I. Introduction

With the development of wireless communications, transmitarrays (TAs) and reflectarrays (RAs) attracted ever-growing attentions [1], [2]. TAs/RAs combine the advantages of lens/reflector antennas and phased array antennas, and thus, have merits of high gain, low cost, and lightweight.

Previous researches mainly focus on improving the performances of TA and RA, such as improving the bandwidth [3], [4], [5], [6], [7], [8], the beam versatility [9], [10], [11], and reconfigurability [12], [13], [14], [15]. However, most of the reported TAs and RAs can only generate a pencil beam toward one direction, which limits their potential applications. Nevertheless, bidirectional antennas are demanded by various wireless systems, such as tunnel relay communications, broadcasting base stations, and interferometric synthetic aperture radars. If multiple antennas are used to fulfill the required bidirectional function, the whole system will be bulky and of high fabrication cost and design complexity. Therefore, considerable efforts have been devoted to combining the TA and RA into one design [16], [17], [18], [19], [20], [21], [22], [23]. In [16], a high-gain bidirectional transmit-reflect-array (TRA) antenna that has a near-zero thickness was proposed. The measured gain of TA and RA is 25.5 and 25 dBi, respectively. However, the transmitted and reflected beams of this design cannot be controlled independently; i.e., the transmitted and reflected beams are symmetric with respect to the planar aperture. In [17], a TRA consisting of four metallic layers and three F4B substrates was proposed. Although it can control the beams of TA and RA independently, the 1-dB gain bandwidth is only 9.14%. For the TRA proposed in [18], the TRA is obtained by using the sparse-array method, of which parts of the elements are transmission elements and the others are reflection elements. Although it can control the beams of TA and RA independently, the 1-dB gain bandwidths of transmission and reflection are only 6.7% and 9.3%, respectively.

Recently, the emerging 3-D printing technology is used to fabricate TAs and RAs to reduce the fabrication cost and provide more design flexibility [24], [25], [26]. In [24], a 3-D-printed dielectric RA was proposed with low cost and high gain at sub-millimeter-wave bands. The 360° phase shift is achieved by changing the height of the 3-D-printed dielectric slab. For the 3-D-printed terahertz TA proposed in [25], the antenna gain ranges from 19.4 to 23.5 dBi within the operating band (50–67.5 GHz). Although these 3-D-printed antennas achieve good RA or TA performances, the transmission and reflection functions have not been achieved simultaneously by a single 3-D-printed antenna.

To solve these issues, a wideband 3-D-printed TRA antenna with transmission and reflection functions depending on the polarization of incident electromagnetic wave is proposed in this communication. The developed TRA element consists of a dielectric post and three copper wires. The phase shift ranges of the proposed element are 450° and 920° for transmission and reflection, respectively, which can be controlled independently by changing the dielectric post height and positions of the copper wires. For the x-polarization incident wave, the transmission function is realized, and the reflection function is achieved for y-polarization waves. Therefore, the proposed TRA can generate two independent forward and backward pencil beams simultaneously by using a dual-linearly polarized horn as the feed antenna. To prove the design concept, a 12 × 12 3-bit TRA is designed, fabricated, and measured. The measured results indicate that the transmission function works within a bandwidth of 46.8% (18–29 GHz) with a maximum gain of 24.4 dBi, and the reflection function operates over a bandwidth of 52.2% (17–29 GHz) with a maximum gain of 22.9 dBi. Moreover, the radiation patterns for both functions are stable over the wide operating bandwidth with a low sidelobe level. These merits make the proposed antenna very suitable for wideband wireless applications where bidirectional beams are required.

Manuscript received 24 August 2022; revised 8 March 2023; accepted 20 March 2023. Date of publication 12 April 2023; date of current version 7 July 2023. This work was supported in part by the National Natural Science Foundation of China under Grant 61801299 and Grant 62071306 and in part by the Natural Science Foundation of Guangdong Province under Grant 2020A1515011037. *(Corresponding author: Long Zhang.)*

Zhenqin Zheng, Long Zhang, and Yejun He are with the College of Electronics and Information Engineering, Shenzhen University, Shenzhen 518060, China (e-mail: zhenqin20@163.com; long.zhang@szu.edu.cn; heyejun@126.com).

Qi Luo is with the School of Physics, Engineering and Computer Science, University of Hertfordshire, AL10 9AB Hertfordshire, U.K. (e-mail: qiluo@ieee.org).

Chunxu Mao is with the Institute for Communication Systems (ICS), 5G Innovation Centre (5GIC), University of Surrey, GU2 7XH Guildford, U.K. (e-mail: c.mao@surrey.ac.uk).

Steven Gao is with the Department of Electronic Engineering, Chinese University of Hong Kong, Hong Kong (e-mail: scgao@ee.cuhk.edu.hk).

Color versions of one or more figures in this communication are available at https://doi.org/10.1109/TAP.2023.3265475.

Digital Object Identifier 10.1109/TAP.2023.3265475

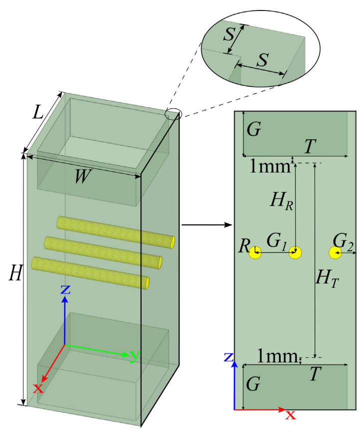

(a) (b)

Fig. 1. Configuration of the proposed TRA element. (a) 3-D view. (b) Side view ($W = L = 7.5$ mm, $R = 0.4$ mm, $G_1 = 2 \times G_2 = 2.5$ mm, $G = 2.8$ mm, $T = 6.5$ mm, and $S = 0.5$ mm).

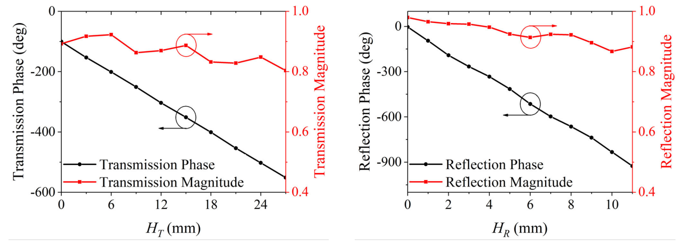

(a) (b)

Fig. 2. (a) Transmission magnitude and phase curves versus H_T at 20 GHz. (b) Reflection magnitude and phase curves versus H_R at 20 GHz.

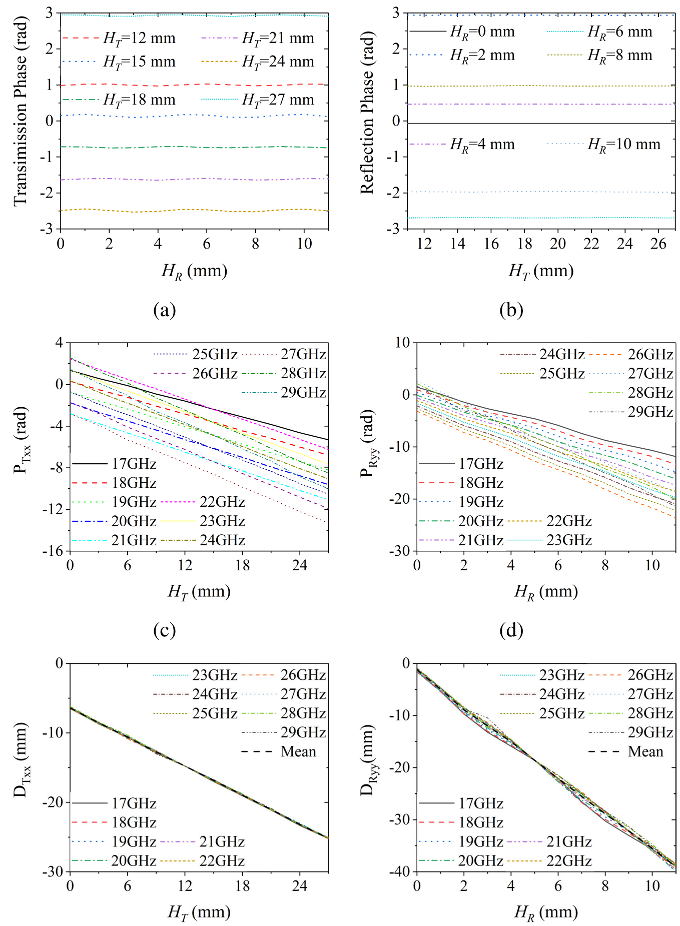

Fig. 3. (a) Transmission phase with different H_R and H_T values. (b) Reflection phase with different H_T and H_R values. (c) $P_{T_{xx}}$ with different H_T values from 17 to 29 GHz. (d) $P_{R_{yy}}$ with different H_R values from 17 to 29 GHz. (e) $D_{T_{xx}}$ with different H_T values from 17 to 29 GHz. (f) $D_{R_{yy}}$ with different H_R values from 17 to 29 GHz.

II. Antenna Design and Operating Principle

A. Design of the TRA Element

The configuration of the proposed TRA element is illustrated in Fig. 1, which is composed of a dielectric post and three copper wires. The dielectric post has a relative permittivity of 2.9 and a loss tangent of 0.0241. Two square holes with a height of G and a width of T located in the upper and lower edge of the dielectric post are used to reduce the reflection caused by impedance mismatch [25]. By adding the square holes at the air–dielectric interfaces, the impedance of the dielectric post changes. Good impedance matching can be achieved by optimizing the width T and the height G of the square holes. Theoretically, the height G should satisfy [25]

$$G = \frac{\lambda_0}{4 \times (\varepsilon_r \times \varepsilon_0)^{1/4}}. \quad (1)$$

In order to minimize the unwanted reflection over the whole operating bandwidth, the optimized parameters are $T = 6.5$ mm and $G = 2.8$ mm.

Three copper wires are placed parallel to the y-axis with a gap of G_1 that is much smaller than the wavelength at 29 GHz. Therefore, the extinction ratio between two orthogonal polarizations becomes quite large below 29 GHz, leading to a good polarizer for the incident wave over a wide bandwidth [27]. Specifically, the x-polarized wave can transmit through the copper wires, so its propagation distance is dependent on the height H. On the contrary, the y-polarized wave will be reflected by the copper wires; thus, the propagation distance of y-polarized wave is determined by the position of copper wires. Tuning the parameter H_T can change H, while tuning the parameter H_R only affects the relative position of the copper wires. Therefore, the propagation distance of the x-polarized and y-polarized waves can be independently controlled by the two parameters H_T and H_R, respectively. It is worth pointing out that the value of H_T must be greater than that of H_R.

The propagation distance of the incident wave is determined by the two geometry parameters H_R and H_T for reflection and transmission, respectively. Therefore, the transmission and reflection performance can be controlled by tuning these two parameters. Fig. 2(a) shows the transmission magnitude and phase shift for the x-polarized wave. As shown, a linear transmission phase response with 450° range is achieved as H_T varies, and the transmission magnitude is greater than 0.8. Moreover, Fig. 2(b) shows that a reflection phase range of 920° is also realized when H_R changes from 0 to 11 mm for the y-polarized wave at 20 GHz. Meanwhile, the magnitude of reflection is greater than 0.86 under all H_R values.

The key factor to realize independent control of reflection and transmission function is to change the reflection phase without affecting the transmission phase, and vice versa. As shown in Fig. 3(a), the transmission phase is nearly unchanged when H_R is changed. Likewise, it can be seen from Fig. 3(b) that changing the H_T barely affects the reflection phase. In other words, these two parameters of the proposed TRA element can independently control the transmission and reflection phase shift.

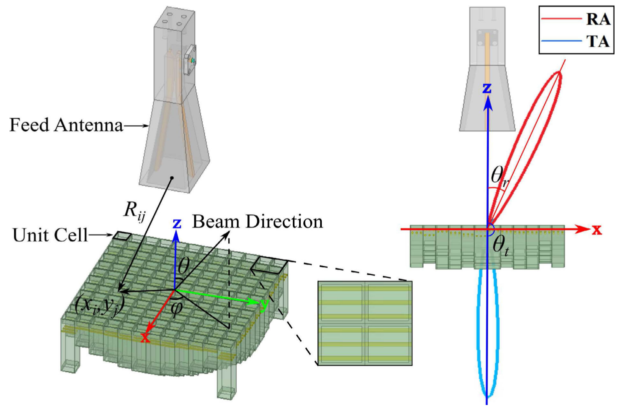

Fig. 4. Configuration of the proposed TRA antenna.

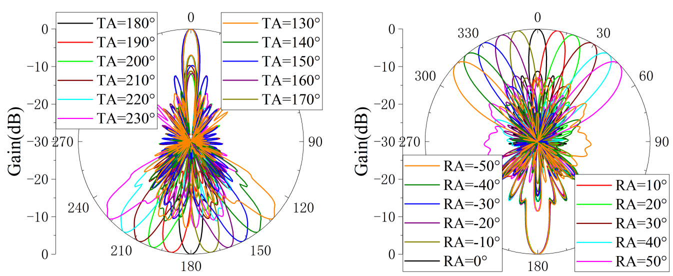

(a) (b)

Fig. 5. Simulation radiation patterns of the TRA antenna. (a) Varying transmitted beam directions while fixing the reflected beams to 0°. (b) Varying reflected beam directions while fixing the transmitted beams to 180°.

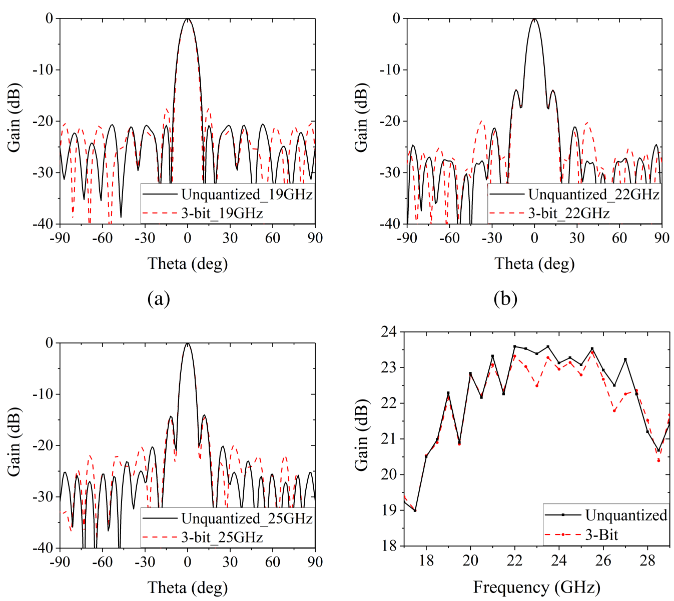

(a) (b) (c) (d)

Fig. 6. Comparison of unquantized and 3-bit quantized TRA. (a) Reflection beams at 19 GHz. (b) Reflection beams at 22 GHz. (c) Reflection beams at 25 GHz. (d) Antenna gain.

The proposed element can realize good reflection and transmission phase characteristics over a wide bandwidth, because the phase shift of the element is realized by changing the propagation distance of transmission and reflection waves, which is similar to the true-time-delay technique [28]. To eliminate the frequency-dependent effect of the element phase shift, the reflection and transmission phase shifts are divided by free-space wavenumber (k_0) [8]

$$D_{T_{xx}/R_{yy}} = \frac{P_{T_{xx}/R_{yy}}}{k_0} \tag{2}$$

where $D_{T_{xx}/R_{yy}}$ and $P_{T_{xx}/R_{yy}}$ refer to the equivalent distance delay and the phase shift of transmission and reflection, respectively. Fig. 3(c) and (d) shows the phase curves of transmission and reflection from 17 to 29 GHz, while the equivalent distance delay of transmission and reflection is shown in Fig. 3(e) and (f). As shown in Fig. 3(e) and (f), the curves of equivalent distance delay for both reflection and transmission are overlapped from 17 to 29 GHz, indicating that the proposed element can compensate the differential spatial phase delay for the proposed TRA over a wide bandwidth [8]. As aforementioned, the proposed element also acts as a wideband polarizer that maintains good reflection and transmission efficiency below 29 GHz. Therefore, a wideband TRA operating from 17 to 29 GHz can be realized by using the proposed element according to the principles of TA/RA antennas [29].

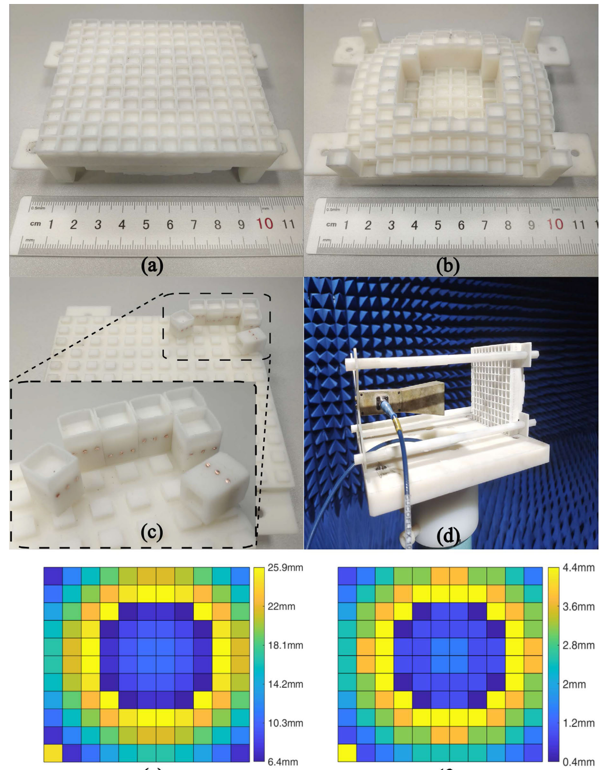

Fig. 7. Fabricated TRA antenna prototype. (a) Front view. (b) Back view. (c) Demonstration of the mortise and tenon joints. (d) Measurement setup. (e) H_T value distribution. (f) 3-bit H_R value distribution.

B. Design of the TRA Antenna

The configuration of the proposed TRA antenna is shown in Fig. 4. A double-ridged horn antenna (DRHA) is used as the feed antenna, which can achieve gain range from 10.14 to 17.16 dBi within a wide bandwidth (10–30 GHz). The DRHA is set with a focal distance of 72 mm (F/D = 0.8). In order to generate beams in the desired direction (θ, φ), the required phase compensation of each element is calculated by

$$\psi(x_i, y_j) = -k((x_i cos\varphi + y_j sin\varphi)sin\theta - R_{ij}) + \phi_0 \tag{3}$$

where (x_i, y_j) is the position of the element, R_{ij} is the spatial distance between the feed antenna and the element, and ϕ_0 is the

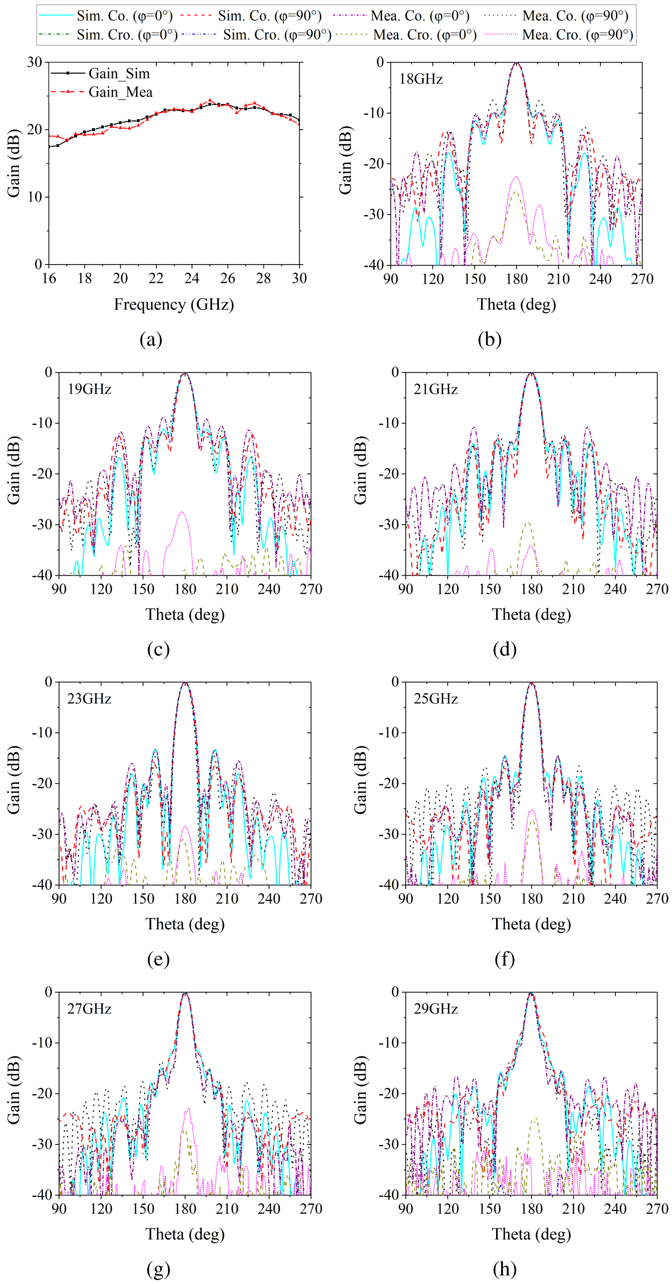

Fig. 8. Gain curves and the radiation patterns of the proposed TRA antenna under transmission function. (a) Gain curves. (b) Radiation patterns at 18 GHz. (c) Radiation patterns at 19 GHz. (d) Radiation patterns at 21 GHz. (e) Radiation patterns at 23 GHz. (f) Radiation patterns at 25 GHz. (g) Radiation patterns at 27 GHz. (h) Radiation patterns at 29 GHz.

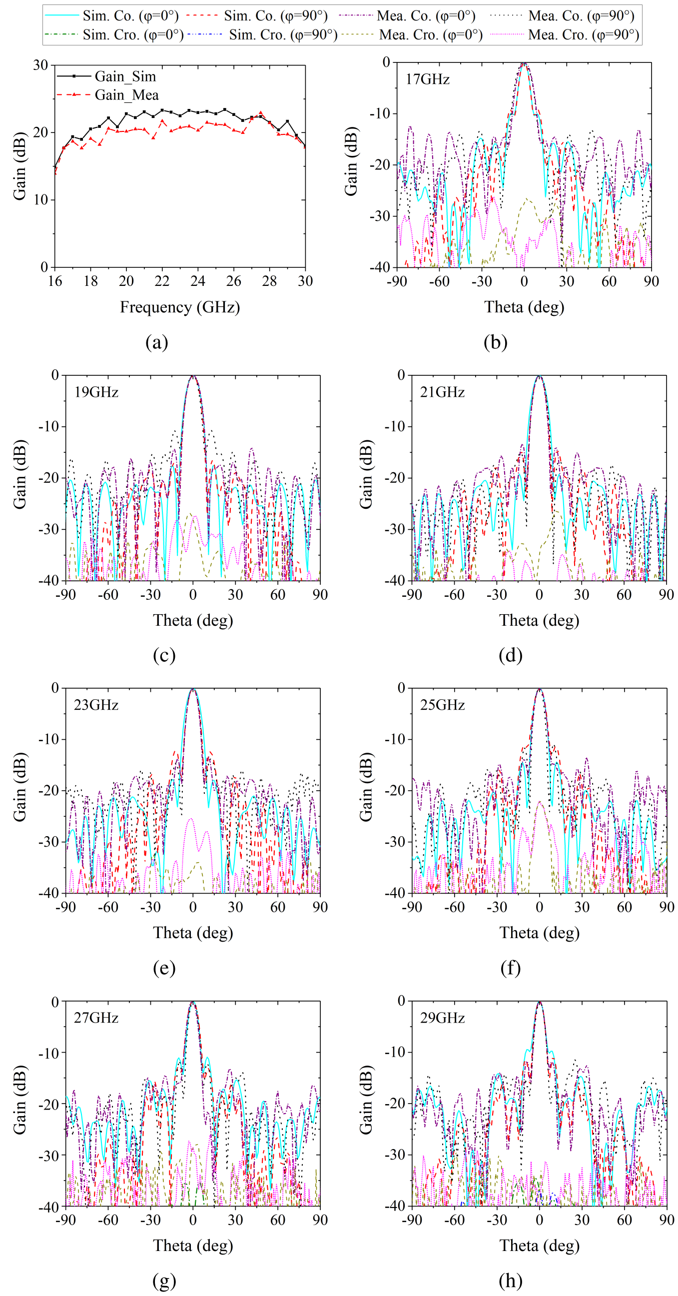

Fig. 9. Gain curves and the radiation patterns of the proposed TRA antenna under reflection function. (a) Gain curves. (b) Radiation patterns at 17 GHz. (c) Radiation patterns at 19 GHz. (d) Radiation patterns at 21 GHz. (e) Radiation patterns at 23 GHz. (f) Radiation patterns at 25 GHz. (g) Radiation patterns at 27 GHz. (h) Radiation patterns at 29 GHz.

initial phase. Using the phase curves of transmission and reflection of the proposed element, the geometry values of each element can be determined according to the phase distributions. Since the value of H_T is greater than that of H_R, it is necessary to calculate the H_R distribution at first. In addition, if the minimum value of H_T is smaller than the maximum value of H_R, appropriate ϕ_0 should be added to the phase compensation of TA to ensure that H_T is greater than H_R.

To verify the independent control of reflection and transmission function, different 16×16 TRA antennas using the proposed element with an aperture size of 120×120 mm are designed. The simulation radiation patterns of the TRA antenna with varied transmission and reflection beam directions are shown in Fig. 5(a) and (b), respectively. As shown by these two figures, the transmitted beam directions can be designed from 130° to 230°, while the reflected beam directions can vary from −50° to 50°. Moreover, the transmission and reflection beams can be controlled independently, as these two beams can be designed separately without affecting each other.

III. Results and Discussion

In order to reduce the difficulty of fabrication, the phase variation of the RA element is quantized to 3 bits. In other words, the H_R values are discrete with only eight values that correspond to the reflection phase shift ranging from 0° to 315° with an interval of 45°.

TABLE I
COMPARISON BETWEEN THE PROPOSED ANTENNA AND REPORTED DESIGNS

Ref.	Peak Gain (dBi) TA/RA	Peak Aperture Efficiency (%) TA/RA	Operational Bandwidth (%) TA/RA	Gain Bandwidth (%) TA/RA	Independent Beam Control (available beam range)	Fabrication Technology
[16]	25.5/25	15/14	15/14 (1-dB gain bandwidth)	15(9.3–10.8 GHz) /14(—) (1-dB)	No	Laser cutting
[17]	21.4/20	36.3/37.4	9.1/11.2 (1-dB gain bandwidth)	9.1(9.4–10.3 GHZ) /11.2(9.3–10.4 GHz) (1-dB)	Yes (—)	3-layers PCB
[18]	21.4/24.4	7/14	6.7/9.3 (1-dB gain bandwidth)	6.7(29.4–31.4 GHz) /9.3(29.1–31.9 GHz) (1-dB)	Yes (—)	3-layers PCB
[19]	24.8/24.3	45.6/48.2	45.2 (3-dB gain bandwidth) /18.6 (1-dB gain bandwidth)	22.6(10.1–12.7 GHz) /18.6(9.3–11.2 GHz) (1-dB)	Yes (—)	4-layers PCB
[20]	27.3/26.2	35.1/48.7	10.4/14.2 (1-dB gain bandwidth)	10.4(12.8–14.2 GHz) /14.2(9.8–11.3 GHz) (1-dB)	Yes (—)	4-layers PCB
This work	**24.4/22.9**	**38.5/28.1**	**46.8/52.2 (Stable radiation pattern bandwidth)**	**32.2(21.4–29.6 GHz) /27.2(21.6–28.4 GHz) (3-dB)**	**Yes(TA:130°–230° /RA: -50°–50°)**	**3D-Printing**

To compare the performance of the unquantized and 3-bit TRA antenna, Fig. 6(a)–(c) presents the normalized radiation patterns of the reflected beams in xoz plane at 19, 22, and 25 GHz. As can be seen from Fig. 6(a)–(c), reflected beams of the unquantized and 3-bit TRA antenna are consistent. The sidelobe levels of the 3-bit reflected patterns are slightly greater than that of the unquantized RA. The gain curves of the unquantized and the 3-bit quantized RA are shown in Fig. 6(d). As shown, the gain difference is small. Therefore, the quantized RA elements will not result in prominent performance degradation to the proposed TRA antenna.

For the convenience of fabrication and measurement, a 12 $\times$ 12 TRA antenna with transmission beam direction of $\theta_t = 180^\circ$ and reflection beam direction of $\theta_r = 0^\circ$ is fabricated using the 3-D printing technology. The accuracy and maximum printable volume of the 3-D printer used are 25 $\times$ 25 $\times$ 100 μm and 145 $\times$ 145 $\times$ 185 mm, respectively. Fig. 7 shows the prototype of fabricated TRA antenna. As shown in Fig. 7(a)–(c), the proposed TRA antenna is assembled using the mortise and tenon joints. More specifically, the whole TRA antenna is divided into two parts for manufacture, as shown in Fig. 7(c). The lower part acts as the base of the antenna and can be used to mount the other part, which consists of elements with different H_R values. Besides, different TAH values can be achieved by 3-D printing the lower part, so there is no need to quantify the H_T value. It is worthwhile to mention that the fabrication tolerance will increase with the increasing number of elements. But, this issue could be alleviated by using multimaterial 3-D printers. Fig. 7(d) shows the measurement setup of the proposed antenna in an anechoic chamber during test. The distributions of H_T and 3-bit H_R values that generate the desired beams are shown in Fig. 7(e) and (f).

For the antenna transmission function, the measured and simulated gain shows small discrepancies, as shown in Fig. 8(a). As shown, a maximum gain of 24.4 dBi is realized at 25 GHz. The simulated and measured radiation patterns are given in Fig. 8(b)–(f), which demonstrate good consistency. The measured results show that stable pencil-shaped beams with cross-polarization level lower than −22.2 dB are achieved across the whole operating bandwidth.

Fig. 9(a) shows the measured and simulated gain of reflection. As shown, a maximum gain of 22.9 dBi is achieved at 27.5 GHz. The discrepancies between simulated and measured reflection gain may result from the blockage of feed antenna, cables, and antenna holder. It can be seen from Fig. 9 that the measured radiation patterns are also in good agreement with the simulated patterns. All the measured SLLs are lower than −10 dB, and all the measured cross-polarization levels are lower than −23.7 dB.

To demonstrate the merits of the proposed TRA antenna, Table I lists the comparison between the proposed antenna and other reported designs. As shown, the proposed antenna can operate over a wider bandwidth, especially for the radiation pattern bandwidth. Moreover, the proposed TRA antenna can generate independent beams for TA and RA functions within a wider bandwidth. Besides, the available beam range for TA function is 130° to 230°, while the beam range for RA function is −50° to 50°, making the proposed TRA more flexible for wide-range signal coverage. In addition, the proposed antenna can be fabricated by low-cost 3-D printing technology, avoiding the usage of multilayer PCB.

IV. CONCLUSION

In this communication, a wideband 3-D-printed TRA antenna is proposed, whose transmission and reflection functions are determined by the polarization of incident wave. The proposed TRA element can control the transmission and reflection phase shift independently within a wide bandwidth, thereby facilitating the independent beam control of the TA and RA functions. A 12 $\times$ 12 TRA is designed, fabricated, and measured. The measured results indicate that the transmission function has a maximum gain of 24.4 dBi with a operating bandwidth of 46.8% (18–29 GHz), and the reflection function has a maximum gain of 22.9 dBi with a operating bandwidth of 52.2% (17–29 GHz). The merits of wide bandwidth, high antenna gain, independent beam control capability, and low fabrication cost make it promising for a variety of wireless applications.

REFERENCES

[1] J. Huang and J. A. Encinar, *Reflectarray Antenna*. Hoboken, NJ, USA: Wiley, 2008.

[2] A. H. Abdelrahman, F. Yang, A. Z. Elsherbeni, and P. Nayeri, *Analysis and Design of Transmitarray Antennas*. San Francisco, CA, USA: Morgan & Claypool, 2017.

[3] M. N. Jazi, M. R. Chaharmir, J. Shaker, and A. R. Sebak, "Broadband transmitarray antenna design using polarization-insensitive frequency selective surfaces," *IEEE Trans. Antennas Propag.*, vol. 64, no. 1, pp. 99–108, Jan. 2016.

[4] T.-J. Li, G.-M. Wang, T. Cai, H.-P. Li, J.-G. Liang, and J. Lou, "Broadband folded transmitarray antenna with ultralow-profile based on metasurfaces," *IEEE Trans. Antennas Propag.*, vol. 69, no. 10, pp. 7017–7022, Oct. 2021.

[5] Z. H. Jiang, F. Wu, T. Yue, and W. Hong, “Wideband and low-profile integrated dual-circularly-polarized transmit-arrays enabled by antenna-filter-antenna phase shifting cells,” *IEEE Trans. Antennas Propag.*, vol. 69, no. 11, pp. 7462–7475, Nov. 2021.

[6] C. Han, Y. Zhang, and Q. Yang, “A broadband reflectarray antenna using triple gapped rings with attached phase-delay lines,” *IEEE Trans. Antennas Propag.*, vol. 65, no. 5, pp. 2713–2717, May 2017.

[7] L. Guo, H. Yu, W. Che, and W. Yang, “A broadband reflectarray antenna using single-layer rectangular patches embedded with inverted L-shaped slots,” *IEEE Trans. Antennas Propag.*, vol. 67, no. 5, pp. 3132–3139, May 2019.

[8] L. Zhang et al., “A single-layer 10–30 GHz reflectarray antenna for the Internet of Vehicles,” *IEEE Trans. Veh. Technol.*, vol. 71, no. 2, pp. 1480–1490, Feb. 2022.

[9] A. Aziz, F. Yang, S. Xu, and M. Li, “A low-profile quad-beam transmitarray,” *IEEE Antennas Wireless Propag. Lett.*, vol. 19, no. 8, pp. 1340–1344, Aug. 2020.

[10] L.-Z. Song, P.-Y. Qin, S.-L. Chen, and Y. J. Guo, “An elliptical cylindrical shaped transmitarray for wide-angle multibeam applications,” *IEEE Trans. Antennas Propag.*, vol. 69, no. 10, pp. 7023–7028, Oct. 2021.

[11] D. Martinez-De-Rioja, E. Martinez-De-Rioja, J. A. Encinar, R. Florencio, and G. Toso, “Reflectarray to generate four adjacent beams per feed for multispot satellite antennas,” *IEEE Trans. Antennas Propag.*, vol. 67, no. 2, pp. 1265–1269, Feb. 2019.

[12] Y. Wang, S. Xu, F. Yang, and M. Li, “A novel 1 bit wide-angle beam scanning reconfigurable transmitarray antenna using an equivalent magnetic dipole element,” *IEEE Trans. Antennas Propag.*, vol. 68, no. 7, pp. 5691–5695, Jul. 2020.

[13] F. Diaby, A. Clemente, R. Sauleau, K. T. Pham, and L. Dussopt, “2 bit reconfigurable unit-cell and electronically steerable transmitarray at Ka-band,” *IEEE Trans. Antennas Propag.*, vol. 68, no. 6, pp. 5003–5008, Jun. 2020.

[14] F. Wu, R. Lu, J. Wang, Z. H. Jiang, W. Hong, and K.-M. Luk, “A circularly polarized 1 bit electronically reconfigurable reflectarray based on electromagnetic element rotation,” *IEEE Trans. Antennas Propag.*, vol. 69, no. 9, pp. 5585–5595, Sep. 2021.

[15] E. Baladi, M. Y. Xu, N. Faria, J. Nicholls, and S. V. Hum, “Dual-band circularly polarized fully reconfigurable reflectarray antenna for satellite applications in the Ku-band,” *IEEE Trans. Antennas Propag.*, vol. 69, no. 12, pp. 8387–8396, Dec. 2021.

[16] F. Yang, R. Deng, S. Xu, and M. Li, “Design and experiment of a near-zero-thickness high-gain transmit-reflect-array antenna using anisotropic metasurface,” *IEEE Trans. Antennas Propag.*, vol. 66, no. 6, pp. 2853–2861, Mar. 2018.

[17] T. Cai, G.-M. Wang, X.-L. Fu, J.-G. Liang, and Y.-Q. Zhuang, “High-efficiency metasurface with polarization-dependent transmission and reflection properties for both reflectarray and transmitarray,” *IEEE Trans. Antennas Propag.*, vol. 66, no. 6, pp. 3219–3224, Jun. 2018.

[18] S. L. Liu, X. Q. Lin, Y. H. Yan, and Y. L. Fan, “Generation of a high-gain bidirectional transmit-reflect-array antenna with asymmetric beams using sparse-array method,” *IEEE Trans. Antennas Propag.*, vol. 69, no. 9, pp. 6087–6092, Sep. 2021.

[19] S. Liu and Q. Chen, “A wideband, multifunctional reflect-transmit-array antenna with polarization-dependent operation,” *IEEE Trans. Antennas Propag.*, vol. 69, no. 3, pp. 1383–1392, Mar. 2021.

[20] X. Liu, Z. Yan, E. Wang, X. Zhao, T. Zhang, and F. Fan, “Dual-band orthogonally-polarized dual-beam reflect-transmit-array with a linearly polarized feeder,” *IEEE Trans. Antennas Propag.*, vol. 70, no. 9, pp. 8596–8601, Sep. 2022, doi: 10.1109/TAP.2022.3161530.

[21] X. Li et al., “Dual-band wideband reflect-transmit-array with different polarizations using three-layer elements,” *IEEE Antennas Wireless Propag. Lett.*, vol. 20, no. 7, pp. 1317–1321, Jul. 2021.

[22] S. Yang, Z. Yan, T. Zhang, M. Cai, F. Fan, and X. Li, “Multifunctional tri-band dual-polarized antenna combining transmitarray and reflectarray,” *IEEE Trans. Antennas Propag.*, vol. 69, no. 9, pp. 6016–6021, Sep. 2021.

[23] J. Zhu, Y. Yang, S. Liao, and Q. Xue, “Dual-band antenna hybridizing folded transmitarray and folded reflectarray,” *IEEE Trans. Antennas Propag.*, vol. 70, no. 4, pp. 3070–3075, Apr. 2022.

[24] P. Nayeri et al., “3D printed dielectric reflectarrays: Low-cost high-gain antennas at sub-millimeter waves,” *IEEE Trans. Antennas Propag.*, vol. 62, no. 4, pp. 2000–2008, Apr. 2014.

[25] H. Yi, S.-W. Qu, K.-B. Ng, C. H. Chan, and X. Bai, “3-D printed millimeter-wave and terahertz lenses with fixed and frequency scanned beam,” *IEEE Trans. Antennas Propag.*, vol. 64, no. 2, pp. 442–449, Feb. 2016.

[26] F. Wei, J.-W. Hao, L. Xu, and X. Shi, “A circularly polarized 3-D printed dielectric transmitarray antenna at millimeter-wave band,” *IEEE Antennas Wireless Propag. Lett.*, vol. 20, no. 7, pp. 1264–1268, Jul. 2021.

[27] J. Ren, H. Wang, W. Shi, and M. Ma, “An ultrawideband polarization-selective reflectarray,” *IEEE Antennas Wireless Propag. Lett.*, vol. 20, no. 12, pp. 2496–2500, Dec. 2021.

[28] E. Carrasco, J. A. Encinar, and M. Barba, “Bandwidth improvement in large reflectarrays by using true-time delay,” *IEEE Trans. Antennas Propag.*, vol. 56, no. 8, pp. 2496–2503, Aug. 2008.

[29] P. Nayeri, F. Yang, and A. Z. Elsherbeni, *Reflectarray Antennas: Theory, Designs, and Applications*. Hoboken, NJ, USA: Wiley, 2018.